

ASCA/ROSAT observations of the radio source MRC 0625–536

C. Otani¹, W. Brinkmann², H. Böhringer², A. Reid³, and J. Siebert²

¹ Cosmic Radiation Laboratory, RIKEN, 2 - 1 Hirosawa, Wako-shi, Saitama 351-01, Japan (otani@postman.riken.go.jp)

² Max-Planck-Institut für Extraterrestrische Physik, Giessenbachstrasse, D-85740 Garching, Germany (wpb@mpe.mpg.de and jos@mpe.mpg.de)

³ School of Physics, The University of Sydney, NSW 2006, Australia (areid@Physics.usyd.edu.au)

Received 9 December 1997 / Accepted 11 August 1998

Abstract. We present the results of ROSAT/ASCA observations of the bright southern radio source MRC 0625–536. The majority of the X-ray emission originates from the surrounding cluster Abell 3391. The best fit temperature for the cluster gas is $kT = 5.8_{-0.3}^{+0.4}$ keV with an abundance of 0.36 ± 0.10 times the solar value. We determined the radial mass profile and extrapolating the data out to 3 Mpc, and we find that the total mass of the cluster is $(0.4 - 1.6) \times 10^{15} M_{\odot}$.

Up to about 10% of the X-ray flux could originate from the central dumbbell galaxy. A comparison of the X-ray contours with the complex 13cm radio structure reveals strong interactions between the radio jets and the surrounding matter.

MRC 0625–536 is thus another object where the interaction between the otherwise invisible matter of the cluster and the activity of the central radio galaxy can be studied by combining data from the radio and the X-ray regimes.

Key words: galaxies: active – galaxies: individual: MRC 0625–536 – X-rays: general – radio continuum: galaxies

1. Introduction

In cross-correlations of the ROSAT All-Sky Survey (RASS) source list (Voges 1992) with radio catalogues impressive correlations were found for quasars and radio galaxies between the (0.1 - 2.4 keV) X-ray luminosity L_x and the monochromatic radio luminosity l_r (Brinkmann et al. 1994 (hereafter paper I), Brinkmann et al. 1995). This suggests a similar origin for the radiation in all radio sources, in accordance with recent unification schemes, which attribute the observed properties of various classes of objects to different viewing angles of the observer with respect to a preferred direction of emission (cf. Orr & Browne 1982, Scheuer 1987, Barthel 1989). In the Molonglo 408 MHz sample (MRC; Large et al. 1981, Large et al. 1991) there is a certain overlap of both object classes, radio galaxies and quasars, at radio luminosities of the order of $l_r \sim 10^{27}$ W Hz⁻¹ (see Fig. 15 in paper I). It appears that objects in that luminosity range still have (in a statistical sense) the average

properties of their classes; there is no smooth transition from one class to the other.

However, due to ROSAT's narrow energy range and its limited energy resolution the spectral properties of the sources are, in general, only poorly determined. These limitations are especially stringent for the discussion of the implications of unification schemes as the data do not seem to support simple orientation-related unification models. We therefore looked with ASCA's superior energy resolution and wider energy range at two sources found in the transition region between radio galaxies and quasars. They are optically classified as galaxies but have X-ray luminosities of the order of 10^{45} erg s⁻¹ comparable to that of low luminosity quasars. Further, the limited spectral information suggested that the central source is intrinsically absorbed, i.e., a quasar nucleus might be buried by dense circumnuclear material.

In this paper we will present the observations of MRC 0625–536 (Large et al. 1981). In the ROSAT Survey the object was a relatively strong X-ray source with a 0.1-2.4 keV X-ray flux of $f_x = 8.1 \times 10^{-12}$ erg cm⁻² s⁻¹ assuming a power law spectrum with photon index $\Gamma = 1.9$ and Galactic absorption ($N_H = 5.4 \times 10^{20}$ cm⁻², Dickey & Lockman 1990). This flux differs slightly from that given in paper I which was obtained from an early version of the RASS processing. Further, the flux is rather uncertain as the source turns out to be extended and does not show a simple power law spectrum (see Sect. 2).

In the radio band the source has been observed over a wide frequency range, from 85.5 MHz to 8.87 GHz. Over this range it has a power-law spectrum ($S \propto \nu^{\alpha}$) with spectral index $\alpha = -1.03$ (A. Burgess, priv. comm.). The source was imaged at 4.8 GHz in 1991 by Gregorini et al. (1994) with the Australia Telescope Compact Array (ATCA), not long after the start of scheduled observations. It shows a possible wide-angle tail morphology with a radio luminosity just below the FR I/FR II break.

Higher dynamic range radio images of 0625–536 were obtained on 1995 January 9 at 20 and 13 cm with the ATCA in the 6A configuration (Reid et al. 1998, in prep). The on-source integration time was 6 hours and the secondary phase calibrator was B0647–475. The 1995 images confirm the FR I/WAT morphology and show that the two jets bend sharply at the outer boundary of the host galaxy. This suggests that the paths of the

radio jets are being strongly influenced by the hot intracluster medium; the source morphology is discussed further in Sect. 3. The total extent is more than 3 arcmin.

The optical counterpart is a pair of interacting galaxies with an extended corona. The redshift of the system, ESO 161–IG 007, is $z \sim 0.0539$ (Teague et al. 1990). The magnitude of the western galaxy is 16.44 and that of the eastern is 15.38 (Danziger & Goss 1983). Tadhunter et al. (1993) detected the Mg I absorption feature, but could not find any emission lines. The optical continuum colors appear bluer than the average early-type galaxy. The position of the radio core coincides with the eastern galaxy. The system was categorized by Gregorini et al. (1992) as a dumbbell galaxy, being the brightest member of the cluster Abell 3391. This cluster has been found to be an X-ray source with a 2–10 keV *Einstein* MPC X-ray luminosity of $2.35 \times 10^{44} h_{50}^{-2} \text{ erg s}^{-1}$ (Edge et al. 1992). The cluster does not show a cooling flow. This is in accordance with the idea that dumbbell galaxies are formed in cluster mergers and that merging clusters do not show cooling flows (McGlynn & Fabian 1984). Further, Teague et al. (1990) claim that A3391 and the cluster A3395, separated by $\sim 1^\circ$ on the sky ($\sim 5 \text{ Mpc}$), together with a compact group of galaxies located midway between the two, form a small super cluster (SC 0627-54).

In this paper we will present the joint analysis of a 20 ks ASCA observation, providing excellent spectral accuracy, and a $\gtrsim 6.6$ ks ROSAT PSPC observation with superior spatial resolution. In Sect. 2 we will discuss the spatial and spectral analysis of the data. In Sect. 3, we will discuss the X-ray data in connection with the recent radio observations obtained with the ATCA. For the derivation of distance dependent quantities we assume for the Hubble constant a value of $50 \text{ km s}^{-1} \text{ Mpc}^{-1}$, which implies that $1'$ corresponds to $\sim 86 \text{ kpc}$ at the distance of A3391.

2. The X-ray observations

Archival data from a $\gtrsim 6.6$ ks ROSAT PSPC observation performed in the beginning of April, 1992 (ROR 800080) were retrieved from the public archive. The ROSAT pointing was not centered on MRC 0625–536 but on the ACO (Abell et al. 1989) position of A3391. A total of ~ 17800 photons were found inside the central $20'$ radius of the detector, containing an extended source and several weaker, unrelated point sources.

MRC 0625–536 was observed with ASCA (Tanaka et al. 1994) in 1994 from November 27, UT 16:04 to November 28, UT 07:04. Both Solid state Imaging Spectrometers, SIS-0(S0) and SIS-1(S1) were operated in 1-CCD Faint mode, and both Gas Imaging Spectrometers GIS-2(G2) and GIS-3(G3) were in normal PH mode. The source center was placed at the so-called “1 CCD nominal position”, which is near the center of S0 chip 1 and S1 chip 3. All data used were selected from intervals of high and medium bit rate. We rejected data at low elevation angles from the earth ($< 5^\circ$) for both SIS and GIS, and from the bright earth ($< 25^\circ$) for SIS. We also rejected the data in the South Atlantic Anomaly for the SIS and the GIS, and the data within 50 sec after each day-night gap of the satellite for the

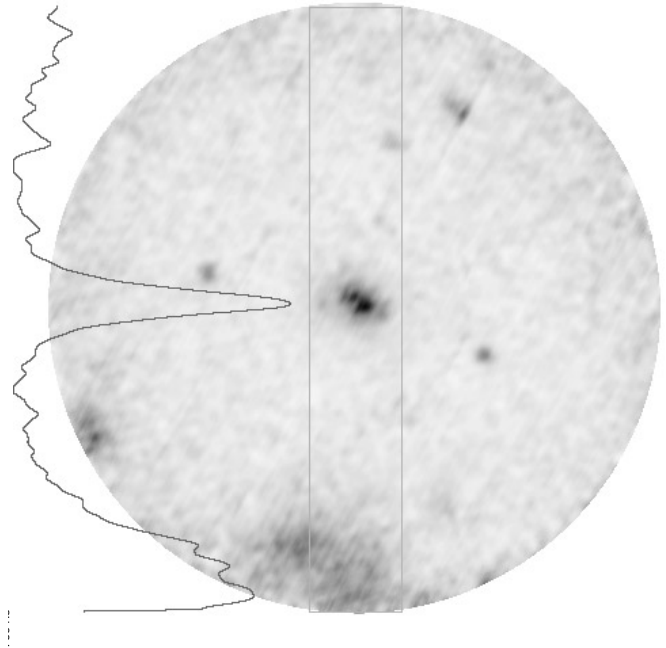


Fig. 1. Exposure corrected X-ray image of the ROSAT pointing showing the innermost $\sim 58'$ radius of the PSPC's field of view. Overlaid is the North-South intensity distribution of a strip $\sim 16'$ wide, centered on the central source.

SIS. Standard corrections for SIS Faint mode data were applied. Hot and flickering pixels were removed in the standard way in the SIS. The usual rise-time screening was applied for the GIS data. The net exposure time was 20.7 ks for the GIS and 16.1 ks for the SIS.

2.1. The ROSAT data

2.1.1. The spatial structure

In Fig. 1 we show the exposure corrected image of the inner $58'$ radius of the PSPC field of view. Clearly visible in the center is the extended emission from the inner parts of the cluster. In the far south we find emission from the central parts of the adjacent cluster Abell 3395. The X-ray emission from this cluster is very diffuse. This is partly due to the fact that there are several components associated with the giant ellipticals dispersed throughout its core, and partly due to the widening of the PSPC's point spread function for sources this far off-axis. Overlaid in the figure is the intensity distribution of a strip ~ 16 arcmin wide, in a north-south direction, indicated in the image. There seems to be enhanced emission between the two clusters, possibly a signature of the super cluster. However, as the southern source is extended, a detailed analysis, taking into account the degrading point spread function towards the outer regions of the PSPC, is required to get a reliable estimate about this contribution.

In Fig. 2 we show an overlay of the most central parts of the X-ray contours onto an optical image, obtained from the digitized sky survey. The contour levels are 3, 5, 8, 16, 32, 48,

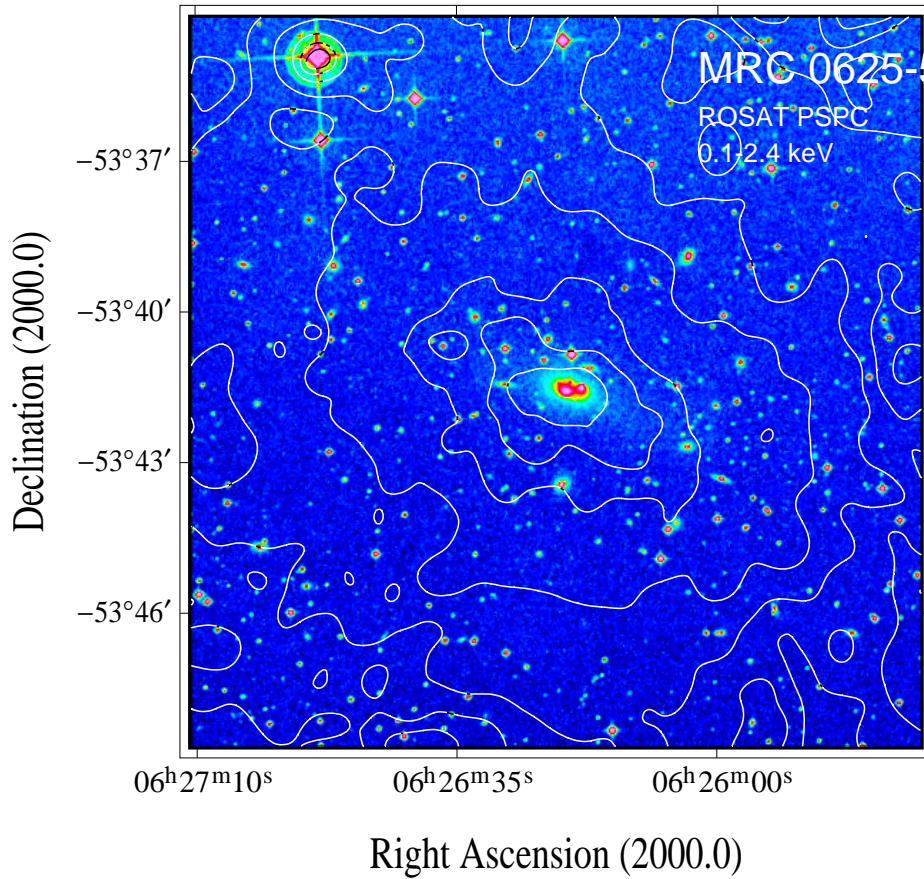


Fig. 2. ROSAT X-ray contours overlaid on a digitized UK Schmidt image. Contour levels are at 3, 5, 8, 16, 32, 48, 64 σ above the local X-ray background. The bright X-ray emitting star seen in the north-east is HD 45844 ($m_V = 9.0$, Olsen 1994).

64 σ above the local X-ray background. The X-ray emission is centered on the central dumbbell galaxy, the highest contour line follows the optical brightness distribution very closely. In general, the bulk of the emission seems to be centered more on the eastern component which is also the host of the radio source and the X-ray emission is clearly extended with a typical size of $\leq 9'$. The X-ray contours show an extension at the same position angle and a similar ellipticity as the optical image with an ellipticity of about 0.7. Details of the structure of the lower contour levels have to be interpreted with care as the data had to be smoothed heavily to overcome the low photon statistics.

2.1.2. ROSAT spectral analysis

The ROSAT observation resulted in a total of ~ 9000 counts from the central 10' radius around the source (including some weaker background point sources) which allow single fits but not a detailed analysis of spectral variations over the extended emission.

Fitting the central region inside a radius of $\sim 10'$ with both a thermal bremsstrahlung spectrum and a Raymond and Smith (RS) emission model resulted in similarly acceptable fits. The thermal bremsstrahlung fit gave a temperature of $kT = 4.03 \pm 2.13$ keV with a reduced $\chi^2_\nu = 0.85$ and the RS model a temperature of $kT = 6.65 \pm 2.74$ keV and a $\chi^2_\nu = 0.89$ (fixing the abundances at 0.35 times the solar value, see

Sect. 2.2). The fitted N_H values are generally slightly lower than the Galactic value. The fitted parameters depend noticeably on the choice of the background, however, the different values always stay inside the 1 σ errors given above.

As the X-ray emission is strongly peaked on the central galaxies we have tried to fit a power law to the data. With the large extraction radius as above no acceptable fit could be obtained. However, for the innermost region of radius 2' centered on the galaxy, an acceptable fit with photon index $\Gamma = 1.67 \pm 0.29$, and $N_H = (6.01 \pm 0.61) \times 10^{20} \text{ cm}^{-2}$ (i.e. higher than the Galactic value) at a $\chi^2_\nu = 0.70$ could be obtained. The corresponding 0.1-2.4 keV flux would then be $f_{\text{pl}} \sim 1.4 \times 10^{-12} \text{ erg cm}^{-2} \text{ s}^{-1}$ resulting in a 'core' galaxy luminosity of $L_x \sim 1.8 \times 10^{43} \text{ erg s}^{-1}$, which agrees well with the average value for radio galaxies detected in the ROSAT band (paper I, Brinkmann et al. 1995).

With increasing extraction radius the fits get worse and, finally, become unacceptable. It should be noted that the fitted power law slope is in good agreement with the average value of $\Gamma \sim 1.8$ generally found for radio galaxies (paper I).

A multi-component fit, consisting of the above (fixed) power law contribution and a free fitted RS model for the whole extended emission resulted in an acceptable fit with $kT = 6.9 \pm 3.7$ keV, $N_H = (4.16 \pm 0.11) \times 10^{20} \text{ cm}^{-2}$ ($\chi^2_\nu = 0.77$). Thus the soft X-ray flux consists mainly of thermal emission from the cluster

gas but we cannot rule out that it contains a smaller (less than 10% at 1 keV) power law contribution from the central source.

2.2. The joint ROSAT and ASCA spectral analysis

While the ROSAT PSPC is operating in the soft, $E \leq 2.4$ keV, energy band the ASCA GIS detector covers the wider, $0.7 \leq E \leq 10$ keV range. Thus a joint fit to the data from both instruments is likely to provide more accurate spectral information. During the ASCA observation of MRC 0625–536 the source intensity was consistent with being constant and flux variations were less than 15%. Therefore, we summed all of the data for the spectral analysis. We extracted the background spectra from the data of a similar observation of MRC 2019+098, because the observed target is extended. The mean count rate was 0.31 cts s⁻¹ for GIS within 6 arcmin and 0.19 cts s⁻¹ for SIS within 3 arcmin.

Although there are indications for a compact source within the extended emission in the ASCA detectors the relatively wide and complex point spread function of the XRT does not allow the discrimination of different components.

We therefore fitted the total emission from the source, using the ROSAT and the ASCA GIS data simultaneously to obtain a maximum bandwidth coverage. As extraction radius we choose for all instruments 10', for the ROSAT data a background field in the outer parts of the PSPC was chosen, a region outside the supposed structure of the super cluster. Within 10' radius, the PSPC count rate was 0.87 c/s and GIS count rate was 0.46 c/s. The normalization factors of the PSPC and the GIS for the Raymond-Smith model coincide surprisingly well within 0.5 % (and the result is the same even if we used the two separate normalizations). Therefore, we used the same normalization in the joint fit of the PSPC and the GIS spectra. In Fig. 3 we show the 1 σ , 90%, and 99% confidence contours for the thermal Raymond-Smith models. Shown are the fitted column densities and the abundances (in units of the solar value) as a function of the temperature.

The best fit obtained ($\chi^2_\nu = 0.656$ for 234 d.o.f) yielded a temperature of $kT = 5.7^{+0.5}_{-0.4}$ keV, an $N_{\text{H}} = 4.6^{+1.4}_{-1.2}$ \times the solar value, where all errors are 90% confidence levels for one interesting parameter (hereafter we use the same definition if not mentioned otherwise). The emission measure of $\langle n^2V \rangle = 2.84^{+0.10}_{-0.08} \times 10^{67}$ cm⁻³ for a distance of 1.05×10^{27} cm implies a (2-10) keV flux of $F_{2-10\text{keV}} = 1.8 \times 10^{-11}$ erg cm⁻² s⁻¹. In particular, the GIS spectrum shows a prominent iron K line at $6.75^{+0.11}_{-0.08}$ keV (in the rest frame) with EW of 400^{+150}_{-150} eV (Fig. 4). In the upper panel of the figure the folded model and the data points are given, in the lower the residuals. Noticeable is the excellent agreement between the two instruments.

The above values for the best fitted spectrum correspond to an absorption-corrected rest frame X-ray luminosity (within a radius of 10 arcmin) of $L_{2-10\text{keV}} = 2.4 \times 10^{44}$ erg s⁻¹. With these values the cluster is an 'average' object with respect to its temperature, X-ray luminosity, and chemical abundances. Its X-ray luminosity is slightly below the well known luminosity -

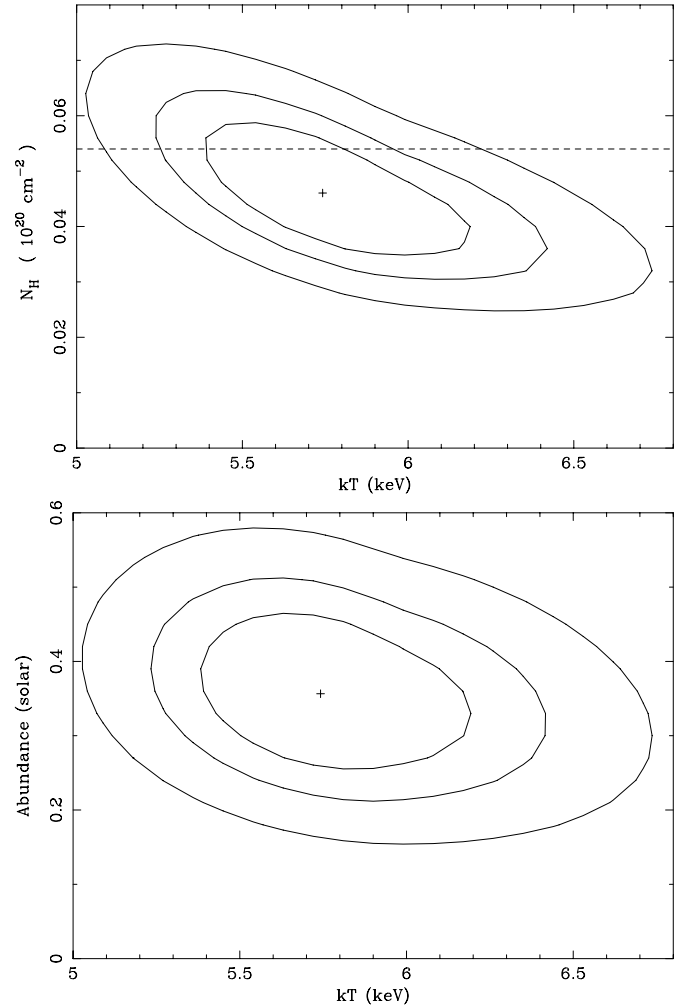


Fig. 3. 1 σ , 90%, and 99% confidence contours of the joint PSPC - GIS fits. Top panel: N_{H} vs kT (the dotted line represents the Galactic N_{H} value); bottom: abundances (in units of solar values) versus kT .

temperature relation $L_x \propto T^{2.79 \pm 0.05}$ (Stewart 1994), but well within the scatter of the data.

To check for possible indications of a cooling flow we tried to fit a cooling flow model to the combined data and obtained a similar χ^2 as above. However, the derived parameters are not well constrained: $kT_{\text{high}} = 6.42 \pm 1.41$ keV, $kT_{\text{low}} = 1.45 \pm 1.98$ keV, an abundance of 0.37 ± 0.09 , and a slope parameter of $s = 1.09 \pm 6.97$. Therefore, this result from the cooling flow model is consistent with that from the RS model. To clarify the contribution from the cooler component we finally explored a two temperature RS model. The addition of the extra low-temperature Raymond-Smith model did not improve the fitting ($\Delta\chi^2 = 1.1$ for two additional parameters). Therefore, we derived the upper-limit of the emission measure of the cooler component by fixing the temperature at the best fit value of 1.45 keV. The upper-limit for the emission measure is then $\langle n^2V \rangle = 5.9 \times 10^{66}$ cm⁻³. Thus, the contribution of the component is less than one fourth of the total component. Note that all other

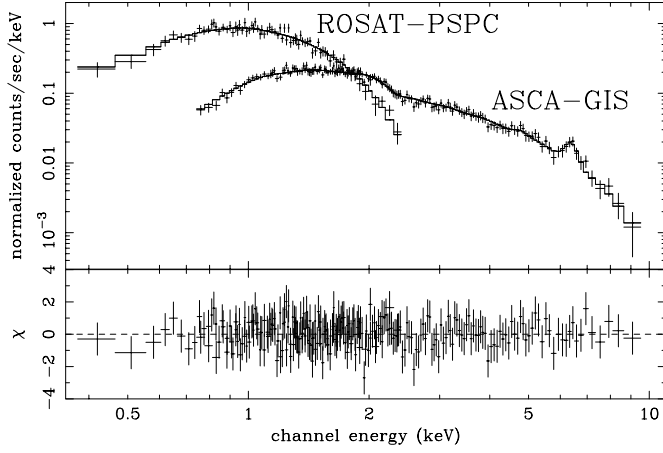


Fig. 4. Joint ASCA GIS - ROSAT fit of a Raymond-Smith model to MRC 0625–536.

parameters are consistent with those for one RS model within the errors.

2.2.1. The cluster analysis

The above results show that the majority of the X-ray emission originates from the cluster Abell 3391. To obtain an approximate description of the X-ray surface brightness distribution, which allows to derive the main physical parameters of the cluster analytically, we use the so called β -model (Gorenstein et al. 1978, Jones & Forman 1984). This describes the surface brightness $S(r)$ of a galaxy cluster assuming spherical symmetry

$$S(r) = S_0 \left(1 + \frac{r^2}{r_c^2} \right)^{-3\beta+1/2} + B \quad (1)$$

where S_0 is the central intensity, r the radius, r_c the core radius, β a slope parameter of the radial surface distribution, and B the background surface brightness. The χ^2 fitting results are: $\beta = 0.56 \pm 0.04$, $r_c = 2.8 \pm 0.5$ arcmin $\equiv 241 \pm 43$ kpc, and $S_0 = 0.0157$ cts s $^{-1}$ arcmin $^{-2}$ cm $^{-2}$ ($\chi^2_\nu = 1.21$). The surface brightness profile and the fit are shown in Fig. 5.

It can be seen that the fitted profile represents the data very well outside a radius of $40''$ (~ 50 kpc). Towards the center there is excess flux due to the emission from the central galaxies.

Fitting this spherically symmetric profile to the image of Abell 3391 has the disadvantage that it does not perfectly describe the slightly elliptical cluster. However, it allows a simple de-projection of the surface brightness profile of the cluster yielding the radial gas density profile. Further, it has been shown (Neumann & Boehringer 1995) that the spherically symmetric approximation is a sufficiently good description for the determination of the gas mass and total mass profiles with errors smaller than relevant uncertainties like those of the temperature distribution in the intra-cluster medium. The analytic de-projection of the profile of Eq. (1) leads to the density profile

$$\rho(r) = \rho_0 \left(1 + \frac{r^2}{r_c^2} \right)^{-3\beta/2}. \quad (2)$$

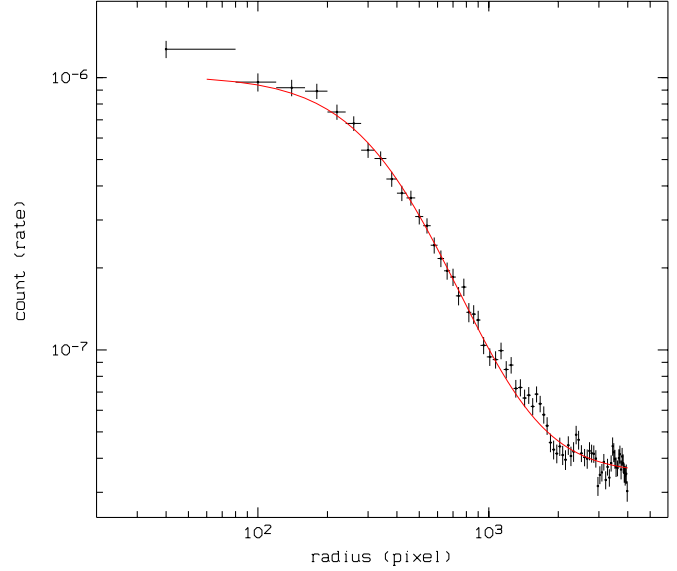


Fig. 5. Surface brightness profile of Abell 3391. The crosses mark the errors and the solid line is the best fit, described in the text. The innermost two data points were excluded from the fit to determine the underlying surface brightness profile without the contribution from the central AGN emission (1 pixel = $0.5''$).

For the central electron density we thus obtain 2.5×10^{-3} cm $^{-3}$ (see Henry et al. (1993) for details).

To check the existence of substructures in addition to the overall ellipticity of the cluster, we produced a synthetic image from the fit parameters and subtracted it from the real image. There is significant substructure, even on smaller scales, at the position of the dumbbell galaxy, and on a larger scales east of the galaxies, as can be seen already in Fig. 7, which shows the original X-ray data. The subtraction of the cluster profile on these scales leads only to a lowering of the X-ray ‘background’.

The data can be used to determine the total and the gas mass of the cluster. The gravitational mass profile can be obtained by combining the isothermal β formalism (equ. 2) with the hydrostatic equation:

$$M(< r) = \frac{kr^2}{G\mu m} \left(\frac{dT}{dr} - \frac{3\beta r T}{r^2 + r_c^2} \right) \quad (3)$$

For the calculation of the gravitational mass profile we take very conservative limits for the temperature range; isothermal models from 5.0 to 6.5 keV with 5.8 keV for the best fitting model. In addition to the isothermal models we also allow for some temperature variation by including polytropic models with polytropic indices ranging from $\gamma = 0.9$ (slightly increasing temperature) to $\gamma = 1.3$ (temperature falling with radius). The same temperature range as for the isothermal models was allowed for the polytropic models with the nominal temperature fixed at the core radius. Fig. 6 shows the obtained results for the gas mass and gravitational mass. For the gravitational mass profile the whole range spanned by the combination of the models is given together with the best fitting isothermal model. It is our experience that this set of mass model families describes the

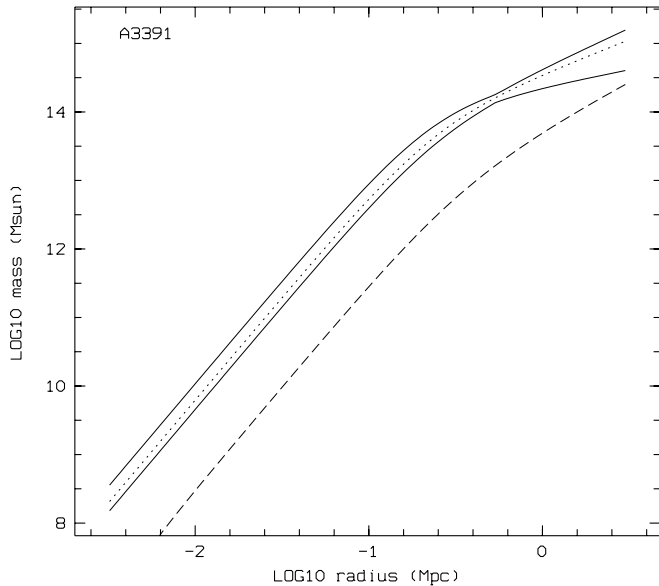


Fig. 6. Integrated mass profile of Abell 3391. The lower, dashed curve gives the gas mass profile determined from the surface brightness profile shown in Fig. 5. The two solid lines give the allowed range of gravitational mass profiles (as determined by polytropic models consistent with the data as described in the text). The dotted line gives the best fitting isothermal model.

expected range of mass profiles very well as shown by a comparison with more sophisticated mass determination methods for objects with better X-ray data (e.g. Neumann & Böhringer 1995, Nulsen & Böhringer 1995).

From these calculations we find for the cluster A3391 a gravitational mass of $(2.3 - 4.5) \cdot 10^{14} M_{\odot}$ and a gas mass fraction of 12 - 24% at 1 Mpc radius. Extrapolating the model to 3 Mpc the mass is $(0.4 - 1.6) \cdot 10^{15} M_{\odot}$ with a gas mass fraction of 16 - 60%. The gas mass fractions are typical for the results found for many galaxy clusters which indicates that the mass determination results are most probably correct. It should be noted that Henriksen & Jones (1996) obtain similar values from an analysis of the ROSAT data alone, based on lower temperatures from the PSPC fit.

3. X-ray - radio comparison

In Fig. 7 we show an overlay of the ATCA 13 cm radio contours on a greyscale image of the central $\sim 4 \times 4$ arcmin of the X-ray emission as measured by the PSPC. The peak of the X-ray emission, centered on the optical position of the eastern galaxy, has a brightness of ~ 1.1 counts per $4'' \times 4''$ pixel, the brighter extended emission about half that value and the fainter ‘background’ ~ 0.21 counts/pixel. The restoring beam used for the 13 cm image was an ellipse with major and minor axes equal to $6.5''$ and $5.0''$, respectively; the major axis position angle is -18.6° .

An inspection of the image reveals some exciting correlations between the structures seen at the two wavelengths. The source appears to emit two oppositely directed jets in approx-

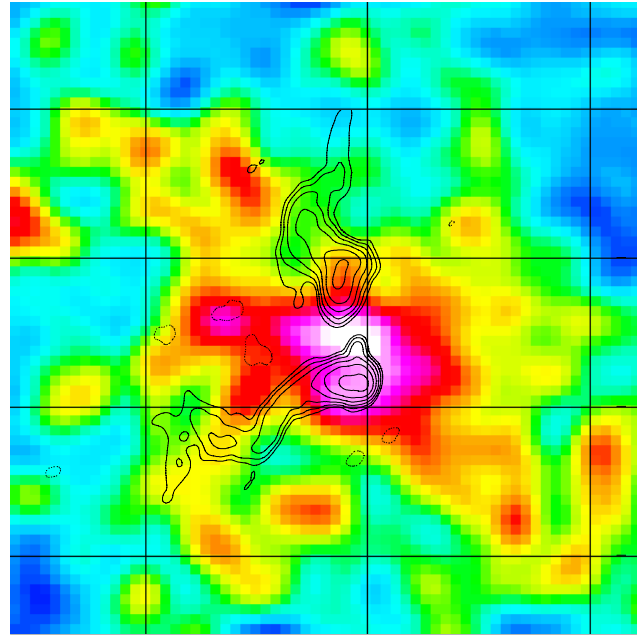


Fig. 7. 13cm ATCA radio contours overlaid on the ROSAT brightness distribution. The peak flux density is 206 mJy/beam, with contour levels at 5, 10, 20, 40, 80 and 160 mJy/beam. The coordinate grid has a spacing of 1 arcmin in declination and 10 s in right ascension. See text for details.

imately a north-south direction. The radio emission originates from the eastern galaxy and the radio ‘core’, which is seen as a weak feature at the northern end of the bright southern lobe, coincides with the optical position of the galaxy. The emission maxima of both lobes, also seen clearly in the 5 GHz image of Gregorini et al. (1994), coincide with regions of higher X-ray brightness - possibly due to inverse Compton emission - and fall outside the optically bright parts of the galaxy. The jets are then deflected, both to the east, by nearly 90° , presumably as a result of pressure gradients or winds in the intracluster medium. Both radio jets seem to ‘escape’ into regions of lower X-ray brightness. The large extent of the X-ray emission, especially to the east, does not have any optical counterpart.

We tried to assess the amount of interaction between the radio jets/lobes and the cluster gas by comparing the pressure of relativistic particles and magnetic fields in the radio-emitting plasma with the pressure of the thermal cluster gas. The latter can be determined directly from the X-ray data and turns out to be in the range $p_{\text{th}} = 4.7 \times 10^{-11} \text{ erg cm}^{-3}$ at the center to $4.1 \times 10^{-11} \text{ erg cm}^{-3}$ at a radius of 100 kpc ($\sim 1.2'$ in Fig. 7). As the radio data are limited we cannot employ the more detailed analysis used, for example, for IC 4296 (Killeen & Bicknell 1988) to obtain the physical parameters of the jets. We thus determine the minimum energy density and pressure p_{eq} for equipartition conditions for Gaussian profile jets using the approach developed by Killeen et al. (1986). Using a code provided by G. Bicknell (priv. comm.) we find that p_{eq} ranges from $\sim 1.6 \times 10^{-11} \text{ erg cm}^{-3}$ at the inner jet to $\sim 6.3 \times 10^{-12}$

erg cm⁻³ along the jet, similar to but slightly lower than the thermal pressure from the X-ray emitting gas.

We thus seem to have another, new example for a jet-gas interaction: previous ROSAT observations of Cygnus A, where the equipartition pressure in the radio hot-spots is higher than the pressure in the cluster gas show strong disturbances of the X-ray profiles by the radio jets (Carilli et al. 1994) and the ‘action’ clearly takes place at the end of the jet. In NGC 1275, which resides at the center of the Perseus cluster, the thermal plasma is displaced by the inner parts of the radio lobes (Böhringer et al. 1993), although the equilibrium pressure in the jets is about a factor of 4 lower than the pressure of the X-ray emitting gas. It was argued that this either implies a deviation from equipartition conditions or a large proton component in the relativistic plasma. Finally, Feretti et al. (1995) and Trussoni et al. (1997) gave examples of associations between radio galaxies and clusters where the gas pressure clearly dominates the pressure in the jets, but these seem to propagate, nevertheless, relatively undisturbed.

Here, we are dealing with a system, where the equipartition pressure seems to be of the same magnitude as the gas pressure. As seen in other cluster WAT sources, the jet propagation appears undisturbed in the central region (within the confines of the host galaxy), but is then massively distorted by material not visible at all, either in X-rays or in the optical. Interestingly, at the positions where the initial jets are stopped and diverted to the east we do not see a high surface brightness in X-rays which would be an indication for a terminal shock of the radio jets. Thus, the mechanism proposed for Cyg A (Carilli et al. 1994) does not seem to apply here.

It should be noted, however, that the analysis of the pressure balance can be biased by projection effects, as the extended radio structures are indeed unusual, and physical distances will in general be larger than projected values. Another uncertainty arises from the numerous physical assumptions used in the calculation of the equilibrium pressure (Killeen et al. 1986). In fact, there is little evidence that the ‘normal’ assumptions actually apply in practice (Killeen et al. 1988; Feretti et al. 1990a, Feretti et al. 1992, Taylor et al. 1994, Röttgering et al. 1994). Higher equilibrium pressures may be obtained if

1. the diffuse emission has a filamentary structure (Hines et al. 1989; Fomalont et al. 1989);
2. a significant amount of energy is in low energy electrons below the adopted low energy cutoff;
3. there is a significant deviation from equipartition; or
4. there is a significant amount of thermal plasma present in the radio plasma, possibly accreted from the ICM (Feretti et al. 1990b).

Furthermore, it is possible that the outer radio structures are not only the result of interaction between radio and thermal plasma, but have an additional intrinsic component, for example due to jet precession. And, finally, it is important to note that the present X-ray image suffers from low photon counts and deeper HRI observations are needed to obtain unambiguous X-ray images.

4. Summary

The radio source MRC 0625–536 is a dumbbell galaxy at the center of the cluster Abell 3391. Most of the X-ray emission from the system originates from the cluster, with only a small fraction $\lesssim 10\%$ attributable to the galaxy itself. This emission is concentrated on the eastern galaxy, which is also the host of the radio emission. Further X-ray emission, east of the galaxies, does not have any obvious optical counterpart. The system seems to be in the process of merging, indicated by the ellipticity of the X-ray emission and by the nature of the central galaxy.

MRC 0625–536 is a very strong radio source with highly distorted oppositely directed jets. The equilibrium pressure of the jets seems to be of the same order of magnitude as the thermal pressure of the cluster gas and there are no indications for the presence of extra matter. Both jets show very similar, pronounced deviations from the initial flow direction. Interestingly, these first large bends of the jets occur roughly in the direction of the supposed merging axis of the cluster, i.e., from south-west to north-east; this is the orientation of the dumbbell system as well as the larger axis of the elliptical X-ray emission. Merger effects have been discussed for clusters with wide-angle tailed radio sources (Gómez et al. 1997), but that sample obviously contains less extreme sources and lower photon statistics in the X-ray images.

In conjunction with previous ROSAT observations of other radio galaxies hosted in clusters, MRC 0625–536 is yet another extreme object where the interaction between the otherwise invisible matter of the cluster and the activity of the central radio galaxy can be studied by combining data from different wave bands, i.e., from the radio and X-ray regimes.

Acknowledgements. The authors thank Richard Hunstead for his assistance with the interpretation of the radio data. The ROSAT project is supported by the Bundesministerium für Bildung, Wissenschaft, Forschung und Technologie (BMBF/DLR) and the Max-Planck-Gesellschaft. WB thanks the Cosmic Radiation Laboratory for hospitality where part of the research was done in the framework of the RIKEN - MPG exchange program. CO is supported by the Special Postdoctoral Researchers Program of RIKEN and thanks the Inter-Research Center Cooperative Program (IRCP) for funding his visit to MPE. HB is supported by the BMBF through the Verbundforschung. ADR acknowledges support from an Australian Postgraduate Award, and from the ASA. This research has made use of the NASA/IPAC Extragalactic Data Base (NED) which is operated by the Jet Propulsion Laboratory, California Institute of Technology, under contract with the National Aeronautics and Space Administration.

References

- Abell G.O., Corwin H.G., Olowin R.P., 1989, *ApJS* 70, 1
 Barthel P.D., 1989, *ApJ* 336, 319
 Böhringer H., Voges W., Fabian A.C., Edge A.C., Neumann D.M., 1993, *MNRAS* 264, 25
 Brinkmann W., Siebert, J., Boller, Th., 1994, *A&A* 281, 355 (paper I)
 Brinkmann W., Siebert J., Reich W., et al., 1995, *A&AS* 109, 147
 Carilli C.L., Perley R.A., Harris D.E., 1994, *MNRAS* 270, 173
 Danziger I.J., Goss W.M., 1983, *MNRAS* 202, 703

- Dickey J.M., Lockman F.J., 1990, *ARA&A* 28, 215
- Duncan R.A., Sproats L.N., 1992, *Proc. ASA* 10, 16
- Edge A.C., Stewart G.C., Fabian A.C., 1992, *MNRAS* 258, 177
- Feretti L., Spazzoli O., Gioia I.M., Giovannini G., Gregorini L., 1990a, *A&A* 233, 325
- Feretti L., Dallacasa D., Giovannini G., Venturi T., 1990b, *A&A* 232, 337
- Feretti L., Perola G.C., Fanti R., 1992, *A&A*, 265, 9
- Feretti L., Fanti R., Parma P., et al., 1995 *A&A* 298, 699
- Fomalont E.B., Ebner K.A., van Breugel W.J.M., Ekers R.D., 1989, *ApJ* 346, L17
- Gómez P.L., Pinkney J., Burns J.O., et al, 1997, *ApJ* 474, 580
- Gorenstein P.D., Fabrikant D., Topka K., Harnden F.R., Tucker W.H., 1978, *ApJ* 224, 718
- Gregorini L., Vettolani G., de Ruiter H.R., Parma P., 1992, *A&AS* 95, 1
- Gregorini, L., de Ruiter, H.R., Parma, P., Sadler, E.M., Vettolani, G., Ekers, R.D., 1994, *A&AS* 106, 1
- Henriksen M, Jones C., 1996, *ApJ* 465, 666
- Henry J.P., Briel U.G., Nulsen P.E.J., 1993, *A&A* 271, 413
- Hines D.C, Owen F.N., Eilek J.A., 1989, *ApJ* 347, 713
- Jones C., Forman W., 1984, *ApJ* 276, 38
- Large M.I., Mills B.Y., Little A.G., Crawford D.F., Sutton J.M., 1981, *MNRAS* 194, 693
- Large M.I., Cram L.E., Burgess, A.M., 1991, *The Observatory* 111, 72
- Killeen N.E.B., Bicknell G.V., 1988, *ApJ* 324, 198
- Killeen N.E.B., Bicknell G.V., Ekers R.D., 1986, *ApJ* 302, 306
- Killeen N.E.B., Bicknell G.V., Ekers R.D., 1988, *ApJ* 325, 180
- McGlynn T.A., Fabian A.C., 1984, *MNRAS* 208, 709
- Neumann D.M., Boehringer H., 1995, *A&A* 301, 865
- Nulsen P.E.J., Boehringer H., 1995, *MNRAS* 274, 1093
- Olsen E.H., 1994, *A&AS* 106, 257
- Orr M.J.L., Browne I.W.A., 1982, *MNRAS* 200, 1067a
- Röttgering H., Snellen I., Miley G., et al., 1994, *ApJ*, 436 654
- Scheuer P.A.G., 1987, In: *Superluminal Radio Sources*, Zensus J.A., Pearson T.J. (eds), Cambridge Univ. Press, Cambridge, p. 104
- Stewart G.C., 1994, in: *Cosmological Aspects of X-Ray Clusters of Galaxies*, W.C. Seitter (ed), Kluwer, Dordrecht, p. 139
- Taylor G.B., Barton E.J., Ge J., 1994, *AJ* 107, 1942
- Teague P.F., Carter D., Gray P.M., 1990, *ApJS* 72, 715
- Tadhunter C.N., Morganti R., di Serego Alighiera S., et al., 1993, *MNRAS* 263, 999
- Tanaka Y., Inoue H., Holt S.S., 1994, *PASJ* 46, L37
- Trussoni E., Massaglia S., Ferrari A., et al., 1997, *A&A* 327, 27
- Voges W., 1992, In: *Proc. of the ISY Conference "Space Science"*, ESA ISY-3, ESA Publications, p.9